scientific reports

Check for updates

OPEN

Structural and molecular differentiation of cultured human neurons is accompanied by alterations of spontaneous and evoked calcium dynamics

Deepika Negi[1], Susan Shorter[1], Iain Goodhall[1], Daniel Razansky[2,3]✉, Sukhi Shergil[4,5] & Saak V. Ovsepian[1,6]✉

During development, neuronal precursors transform from a pluripotent state into specialized neurons. While much research has been conducted into morphological and molecular changes, there is a pressing need to define accompanying functional alterations. We used immunofluorescence microscopy and live imaging in SH-SY5Y-derived human neurons to elucidate the relationship between structural and molecular differentiation with evoked and spontaneous Ca^{2+} dynamics. In the undifferentiated state expressing trace amounts of neuronal markers, SH-SY5Y cells maintain spontaneous high-amplitude slow Ca^{2+} oscillations, with their stimulation by carbochol activating low-amplitude Ca^{2+} transients. Driving SH-SY5Y cells into the 2CL state by retinoic acid facilitated the outgrowth of neurites and expression of neuron-specific proteins. These changes are accompanied by the abolition of Ca^{2+} oscillations. Differentiating SH-SY5Y cells into definitive neurons by a cocktail of retinoic acid and BDNF induced their polarization and enrichment with specific neuronal markers, accompanied by a resurgence of spontaneous Ca^{2+} oscillations but with faster kinetics. The carbachol-induced rise of Ca^{2+} in these cells showed a higher peak and biphasic decay. At all developmental stages, Ca^{2+} transients in response to ionomycin were indistinguishable. These findings lead us to conclude that a switch of Ca^{2+} dynamics accompanies structural and molecular differentiation of SH-SY5Y cell-derived human neurons, contributing to the developmental process.

Keywords Neuroblastoma-derived neurons, BDNF, Calcium imaging, Spontaneous activity, Molecular polarization, SH-SY5Y cells

The conservation of biological processes and mechanisms across various species, safety and ethical considerations, improvements in transgenic tools and increasing affordability have contributed to the growing use of animal models in translational biomedical research[1,2]. The principal disadvantage is that animal studies fail to capture faithfully the complexity of human conditions and disease mechanisms[2,3]. Over the recent decade, there has been a growing interest in utilizing human cells and tissue in biomedical research, with increasing applications of progenitor cells from embryos[4] and stem cell-derived models[5]. Indeed, studies in human cell cultures provide a better approximation of molecular biology and genetics of human diseases and development, with excellent control of experimental conditions and accessibility[6]. The principal downside of these models is that they are overly simplified and come with ethical issues related to the use of human material, along with potential legal and regulatory challenges[7,8]. Furthermore, the research involving human pluripotent stem cells (hPSCs) and induced PSC-derived models is labour-intensive and expensive[9].

[1]Faculty of Engineering and Science, University of Greenwich London, Chatham Maritime, London ME4 4TB, UK. [2]Faculty of Medicine, Institute of Pharmacology and Toxicology and Institute for Biomedical Engineering, University of Zurich, Zurich, Switzerland. [3]Department of Information Technology and Electrical Engineering, Institute for Biomedical Engineering, ETH Zurich, Zurich, Switzerland. [4]Department of Psychosis Studies, King's College London, Institute of Psychiatry, Psychology & Neuroscience, London, UK. [5]Kent and Medway Medical School, Canterbury, UK. [6]Faculty of Medicine, Tbilisi State University, Tbilisi 0177, Georgia. ✉email: daniel.razansky@uzh.ch; s.v.ovsepian@gre.ac.uk

Immortalized human cell lines have attracted interest as potential alternatives, with increasing numbers of reports using NT2, PC12, N1E-115, NG108-15, and SH-SY5Y cell lines to address a range of mechanistic and translational questions[10–14]. Robustness, affordability, and genetic continuity have made some of these lines attractive to the field of neuroscience research. Derived from the SK-N-SH progenitor of a bone marrow biopsy of the neuroblastoma of a child, the immortalized SH-SY5Y line is widely used to address a range of neurochemical[15,16], molecular[16–18] and developmental[19] neurobiology and translational questions[20,21]. In cultures, these cells show excellent viability and can be readily induced into neurons, exhibiting characteristic morphological and neurochemical phenotypes[17,18,22]. SH-SY5Y cells are robust, sustain homogeneity, differentiate into several neuron types if conditions are favourable, and can be maintained at low costs[17,23]. Commercial accessibility of human SH-SY5Y cells eliminates ethical or legal hurdles, making the cell line one of the most widely used in vitro neuronal models[17,18,24,25].

Developmental studies demonstrated reliable sequential differentiation of SH-SY5Y cells into morphologically, neurochemically and molecularly mature neurons[17,18,24]. Analysis of markers confirms their acquisition of dendrites and axons, which form specialized synaptic contacts[17,26]. There is, however, a significant gap in functional data and demonstration of activity dynamics of SH-SY5Y cells during differentiation[27]. Since neuronal development and wiring entail complex electrical and neurochemical activity and intercellular signaling, it is critical to elucidate the functional alterations of developing SH-SY5Y cells to relate structural and molecular changes with underlying processes and mechanisms[28]. Calcium imaging has proven highly instructive, with spontaneous and evoked transients measuring neuronal excitability and various activity states. The dynamics of Ca^{2+} play a pivotal role in multiple signaling processes, regulating differentiation and developmental mechanisms, cellular homeostasis and plasticity[29,30].

In this study, we combined immunofluorescence confocal microscopy with live Ca^{2+} imaging of sequentially differentiating SH-SY5Y cell-derived human neurons[17,18,23] to elucidate the relationship between evoked and spontaneous calcium dynamics with structural and molecular transformation of the progenitors into mature neurons. The rationale for analyzing various differentiation stages is to determine the dynamics and relationship of functional changes associated with transformation of SH-SY5Y cells into neurons exhibiting distinct molecular and morphological characteristics.

Materials and methods

Materials and reagents

SH-SY5Y cell line (CRL-2266, ATCC), Dulbecco's modified eagle medium (DMEM, Thermo 41965-039), neurobasal-A (10888022 Thermo), N2 (11520536 Thermo), trypsin (25200056 Thermo), fetal bovine serum (16000044, Thermo), mounting media with DAPI (F6057 Sigma), penicillin streptomycin solution (P0781 Sigma), phosphate buffered saline (PBS, 18912014, Thermo), L-glutamine (25030032, Thermo) Nunc™ cell-culture treated multi-dishes (140675, Thermo), T-25 cell-culture treated flask (156367, Thermo), DMSO (32160405, Sigma), paraformaldehyde 16% (043368.9 L Thermo), carbachol (C4382-1G Sigma), ionomycin (124222 Thermo), brain derived neurotrophic factor (BDNF, 248-BDB-010/CF, Biotechne), retinoic acid (RA, 0695/50 Biotechne), Corning® Costar™ 24-well clear TC-treated multiple well plates (10380932, Fisher Scientific).

Culturing and differentiation of neuroblastoma cells

The frozen SH-SY5Y cells from ATCC were thawed in T25 culture flasks in a standard growth medium containing DMEM. The flusk media of all cells utilized for structural and molecular differentiation studies were supplemented with 10% FBS (Table 1); the media of cells cultured for live imaging experiments was supplemented with 15% FBS (Table 2). Both groups also contained 1% ATB and were maintained at 37 °C in 5% CO_2. Upon reaching 80–90% confluence, cells were treated with a trypsin-EDTA solution, plated at the desired seeding density and split into multiple groups (Tables 1 and 2), with cell counting made using a haemocytometer.

As detailed in Tables 1 and 2 and discussed in our earlier report[17], at day 0, SH-SY5Y cells were seeded at a 100,000-cell density per well in 24-well polymer plates in the medium containing DMEM[31]. Cultures were maintained at 37 °C with 5% CO_2. We set up three groups of cultures for studying morphological and molecular differentiation (Table 1) and four groups for live calcium imaging (Table 2). The first group includes (1) control cultures of undifferentiated SH-SY5Y cells in DMEM with gradual FBS withdrawal from 5 to 0.5% with 1% ATB over 12 days; (2) RA-treated SH-SY5Y cells exposed to RA (10μM) in DMEM medium with FBS starvation from 5 to 0.5% over 12 days in the presence of 1% ATB and (3) RA + BDNF-treated SH-SY5Y cells exposed to a RA (10μM) for 6 days in DMEM medium with gradual FBS withdrawal from 5 to 2% for 6 days, followed by addition of BDNF (50ng/ml) for 6 days in Neurobasal medium supplemented with 1% N2, L-glutamine (2mM) and 1% ATB (Table 1)[17]. The second group set for calcium imaging, we compared actively proliferating

Group/Day	Day 0	Day 1	Day3	Day 6	Day 9	Day 12
Control FBS starved	DMEM + 5% FBS + 1% ATB	DMEM + 5% FBS + 1% ATB	DMEM + 2% FBS + 1% ATB	DMEM + 0.5% FBS + 1% ATB	DMEM + 0.5% FBS + 1% ATB	Fixation
RA- differentiated cells	DMEM + 5% FBS + 1% ATB	DMEM + 5% FBS + 1% ATB + 10μM RA	DMEM + 2% FBS + 1% ATB + 10μM RA	DMEM + 0.5% FBS + 1% ATB + 10μM RA	DMEM + 0.5% FBS + 1% ATB + 10μM RA	Fixation
RA-BDNF differentiated cells	DMEM + 5% FBS + 1% ATB	DMEM + 5% FBS + 1% ATB + 10μM RA	DMEM + 2% FBS + 1% ATB + 10μM RA	NB + 1% N2 + 1% ATB + 2mM L-glutamine + 50ng/ml BDNF	NB + 1% N2 + 1% ATB + 2mM L-glutamine + 50ng/ml BDNF	Fixation

Table 1. Representation of the 12-day timeline of differentiation of SH-SY5Y cells used for immunostaining, with details of experimental conditions.

Group/ Day	Day 0	Day 1	Day3	Day 6	Day 9	Day 12
Control 15% FBS	DMEM + 15% FBS + 1% ATB	DMEM + 15% FBS + 1% ATB	DMEM + 15% FBS + 1% ATB	DMEM + 15% FBS + 1% ATB	DMEM + 15% FBS + 1% ATB	Live Ca^{2+} imaging
Control FBS Starved	DMEM + 5% FBS + 1% ATB	DMEM + 5% FBS + 1% ATB	DMEM + 2% FBS + 1% ATB	DMEM + 0.5% FBS + 1% ATB	DMEM + 0.5% FBS + 1% ATB	Live Ca^{2+} imaging
RA- differentiated cells	DMEM + 5% FBS + 1% ATB	DMEM + 5% FBS + 1% ATB + 10 µm RA	DMEM + 2% FBS + 1% ATB + 10 µm RA	DMEM + 0.5% FBS + 1% ATB + 10 µm RA	DMEM + 0.5% FBS + 1% ATB + 10 µm RA	Live Ca^{2+} imaging
RA-BDNF differentiated cells	DMEM + 5% FBS + 1% ATB	DMEM + 5% FBS + 1% ATB + 10 µm RA	DMEM + 2% FBS + 1% ATB + 10 µm RA	NB + 1% N2 + 1% ATB + 2mM L-glutamine + 50ng/ml BDNF	NB + 1% N2 + 1% ATB + 2mM L-glutamine + 50ng/ml BDNF	Live Ca^{2+} imaging

Table 2. Representation of the 12-day timeline of differentiation of SH-SY5Y cells used for the calcium imaging experiment with details of experimental conditions.

cells maintained in 15% FBS, with FBS-starved controls, RA and RA-BDNF groups (Table 2). The adopted experimental protocol enables the determination of the effects of FSB starvation and differentiation of SH-SY5Y cells into neurons on Ca^{2+} dynamics. Experiments were conducted in triplicate with conditions kept consistent to ensure reproducibility of the results.

Immunofluorescence staining of neuroblastoma cells

On day 12, cells were washed three times in 24-well plates with phosphate-buffered saline pH 7.4 (1X PBS) and fixed using 4% PFA in 1X PBS for 20 min, followed by 3 × washes with PBS and permeabilized with 0.1% Triton X-100 in 1X PBS for 10 min at room temperature. The step was followed by 3 × washes with PBS and binding by 2% FBS in PBS for 1 h at RT. Fixed cells were then incubated overnight with primary antibodies at 4 °C, which were subsequently removed, and after 3 × washes, treated with secondary antibodies overnight at 4 °C. Afterwards, secondary antibodies were removed, and cells were washed 3 × with PBS, followed by covering with a mounting medium containing nuclear stain DAPI. After drying and cover slipping, the samples were viewed with a Confocal (ZEISS LSM 880) microscope in epifluorescence mode. Confocal images were acquired on the same microscope in laser scanning mode with a 40 × NA = 1.3 oil immersion Zeiss objective. All experiments were conducted in triplicate, with conditions kept constant. For excitation of fluorescent-labelled secondary antibodies, we used 488 nm (Tau and PSD95), 568 nm (BT and Synapsin) and 647 nm (Map2) laser lines with images sampled in the same mode at a spatial resolution of 30 nm per pixel and dwell time of 1.5 µs.

Live calcium imaging

On day 12 (Table 2), the media of cell cultures were replaced with Fluo-4 (2µM) containing media for 30 min before imaging. After washing cells with PBS, fresh Fluo-4-free media was added, and the plates were mounted on the microscope stage for live Ca^{2+} imaging inside the imaging chamber with a controlled environment. Micrographs were captured in time series mode at 1 Hz on ZEISS LSM 880 confocal laser scanning microscope with a 40 × oil immersion objective. A 488 nm laser was used for excitation of the fluorophore. In experiments that monitored spontaneous Ca^{2+} oscillations, recordings were made continuously for over 400 s without stimulants. In studies of evoked Ca^{2+} transients, all conditions were kept the same except that after collecting 100 frames, cholinergic agonist carbachol (50 µM)[32] or Ca^{2+} ionophore ionomycin (5 µM)[33,34] was added, followed by recording over 300 s. All collected data were analyzed offline using Image-J (NIH Image-J, Version Win64). Data processing and analysis were carried out using IBM SPSS Statistics software (Version v29.0.1.0). Analysis of the frequency of spontaneous Ca^{2+} oscillations and amplitude-kinetic parameters of the evoked Ca^{2+} transients was carried out using Easy Electrophysiology software (https://www.easyelectrophysiology.com/) in semiautomatic or automatic modes. Individual transients of Ca^{2+} were detected by setting an empirical threshold to capture events exceeding the baseline noise intensity deviations by a factor of 3[35]. The reliability of the detection of individual events was verified manually and compared with that of those detected using a threshold-based algorithm.

Image processing, data analysis and presentation

Experimental data were collected from triplicate studies. Sholl analysis was used to count systematically the number of neurites and their branches as reported in our earlier paper[36]. The number of putative synaptic contacts was counted manually over normalised areas within 15–50 µm range of the soma. For fluorescence intensity measurements, we used multiple regions of interest (ROIs), with numerical values extracted for offline analysis with IBM SPSS. A similar approach was used for colocalization analysis, applying ImageJ JACoP colocalization plugin. All numerical values (i.e. Pearson's correlation coefficient and Mander's colocalization coefficient) were extracted and analyzed offline using IBM SPSS Statistics software. The results are presented as mean SE, with the statistical significance determined using Student's *t*-tests or Tukey's post hoc tests, with $p < 0.05$ defined as significant. Figures were prepared using Adobe Illustrator Artwork 16.0 in the Adobe Creative Suite Version 6 program. EndNote X8.2 was used for reference formatting per journal guidelines.

Results

General characterization of SH-SY5Y cell cultures

SH-SY5Y cells were maintained under different conditions to induce various developmental stages of neurons for morphological, molecular and functional studies (see Methods and Tables 1 and 2). Cultures retained in control media are taken as non-differentiated controls. RA treatment of SH-SY5Y cells induced the differentiation process, leading to morphological changes like neurite outgrowth and a decrease in cell proliferation[15,17,23,37].

These alterations result from activation of retinoic acid receptors and their downstream targets, promoting the development of neuron-like phenotypes. Finally, exposure of cultures to a cocktail of RA with BDNF has been reported to promote the development of specific neuronal characteristics such as differentiation of neurites into axons and dendrites and formation of synaptic contacts[17,18,23,37,38].

For structural analysis of cultures at different stages of differentiation, they were fixed with PFA and imaged in brightfield mode. Figure 1 summarises the results of these studies. Cultures maintained for 12 days in control media (Table 1) display large and irregular soma with sparse and short processes. Most cells in these cultures assemble in dense groups, indicating their active proliferation state (Fig. 1A1 and A2). Cultures treated with RA for 12 days exhibited smaller soma with distinctly elongated processes making occasional contacts (Fig. 1B1, Fig. 2). Finally, cells in cultures after 6 days of RA treatment exposed to RA + BDNF for six additional days showed the morphology of a typical neuron with more regular shape of soma, extensive branching of processes, which formed numerous contacts and varicosities (Fig. 1C1, Fig. 2). The results of counting the neurites and the number of contact points over normalized areas are summarized in (Fig. 1D–F). As can be seen, the control group developed fewer outgrowths per soma, whereas in RA and, especially, RA + BDNF group, the number of neurites per soma increased significantly (Fig. 1D). The higher incidence of neurite crossover in RA-BDNF differentiated cultures was subject to further analysis. Counting the number of contacts within randomly defined ROIs (15–50 m range of the soma) showed that the number of contacts is highest in cultures treated with RA + BDNF (× 20 controls) followed by RA (× 4 controls) treated cultures (Fig. 1E). Analysis of the relationship between the number of neurites and contacts showed a weak but significant correlation in control cultures.

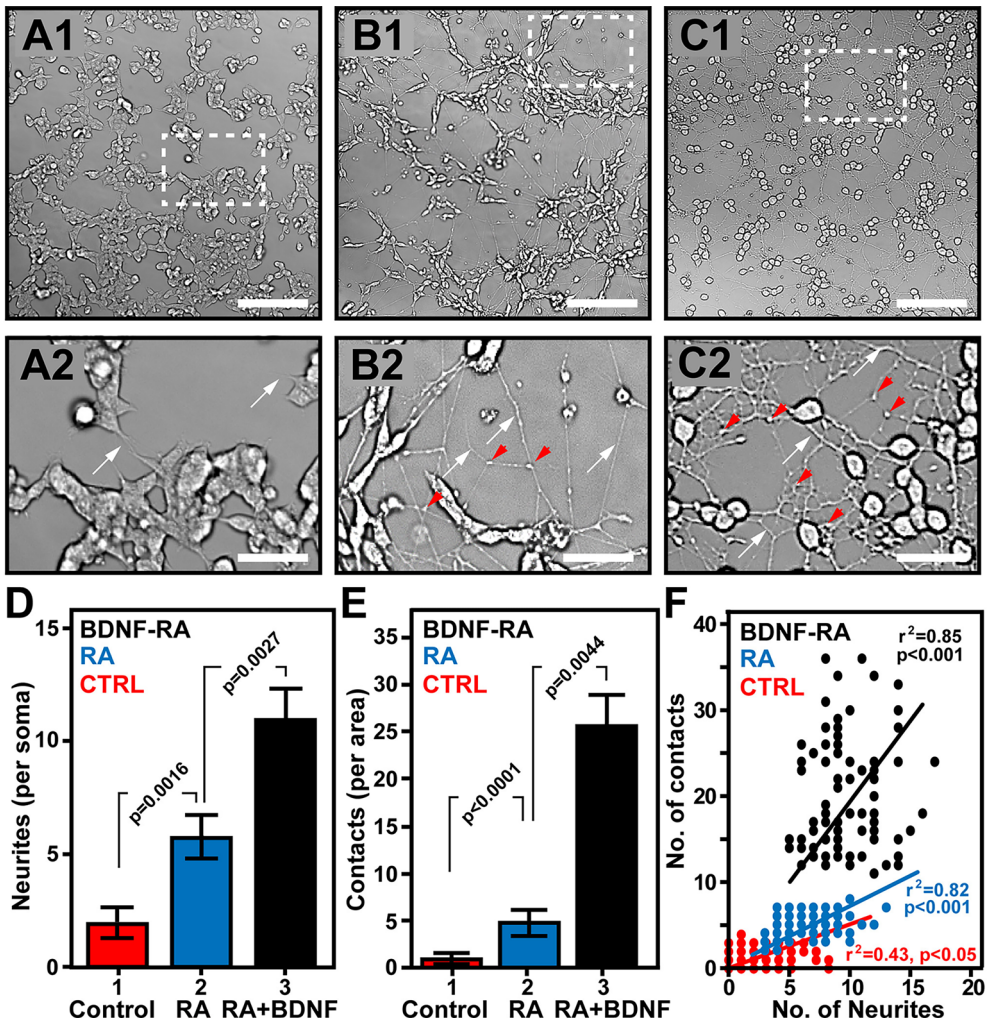

Fig. 1. Morphological characterization of SH-SY5Y cell cultures. (**A1**–**C2**) Typical brightfield images of 12-day-old Control (**A1-2**), RA (**B1-2**) and RA + BDNF (**C1-2**) cultures. The top row has a wide field of view; the bottom row has an expanded view of boxed areas (dashed boxes). White arrows point to neurites; red arrowheads point to putative contacts. Scale bars top, 250 µm, bottom 40 µm). (**D**,**E**) Summary histograms of the number of neurites per soma and number of contacts over normalised areas, respectively, in Control, RA and RA + BDNF cultures. Histograms show means and ± SEM. $N = 100$ per group, three replicas. (**F**) The scatter plot shows the relationship between the number of contacts and the number of neurites per cell in Control, RA and RA + BDNF cultures.

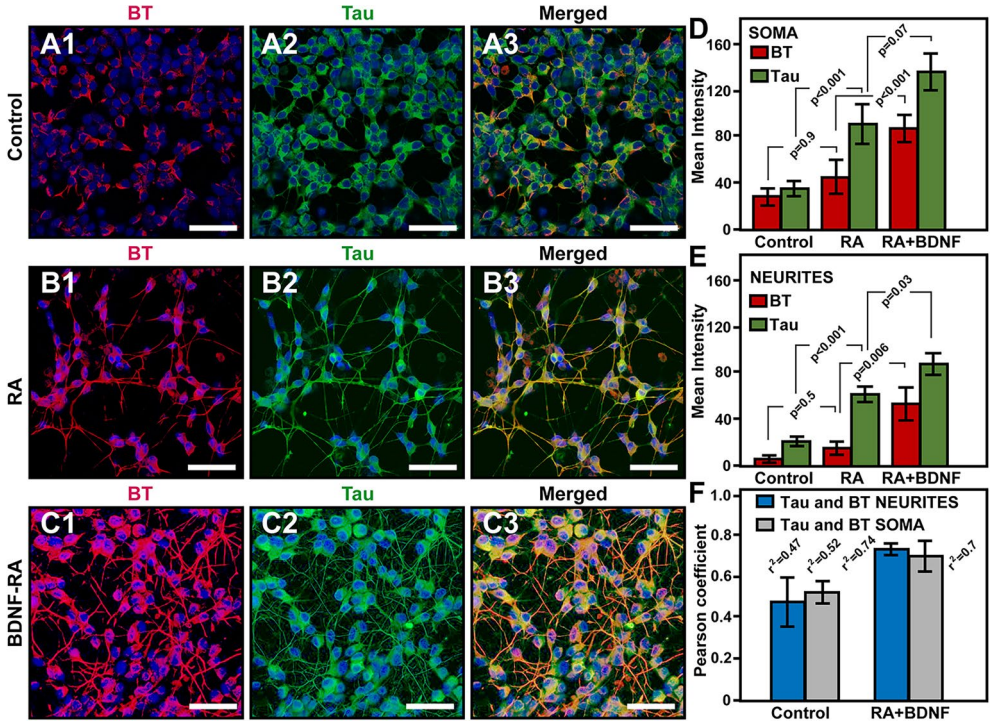

Fig. 2. BT–Tau expression and distribution in SH-SY5Y cell cultures. (**A1**–**C3**) Typical confocal immunofluorescence micrographs of 12-day-old Control, RA and RA + BDNF cultures stained for β-tubulin (BT) and Tau protein (red and green, respectively). Blue - counterstaining of cells with DAPI. Scale bars: 80 μm. (**D**,**E**) Summary histograms of the intensity of staining for β-tubulin and Tau protein (red and green, respectively) in soma and neurites (SOMA and NEURITES) showing the distribution of signal intensity in Control, RA and RA + BDNF cultures. Histograms show ± SEM. $N = 30$ ROI per group, three replicas. (**F**) The bar graphs show the Pearson correlation values of β-tubulin and MAP2 protein in soma and neurites of control and RA-BDNF differentiated cells. Test for the significance of the relationship between two variables of each dataset with a paired Student t-test produced $p < 0.05$ for all datasets.

In RA and RA-BDNF-treated cultures, however, the correlation between these two variables was stronger and highly significant (Fig. 1F).

Dynamics of structural proteins at various stages of developing SH-SY5Y cells

Next, we performed the immunostaining of SH-SY5Y cells at different developmental stages for generic and specific neuronal proteins. As above, after reaching the desired differentiation stages, cultures were fixed but stained for axonal tau, dendritic MAP-2 and skeletal protein β-tubulin[39–41]. The preparation of cells for staining was as described above (see Methods). Signal intensity and colocalization analysis were carried out using intensity or colocalization plugins of Image-J. Figure 2 shows representative micrographs and summarises the results of intensity and colocalization studies. Comparison of staining of three sets of 12-day-old undifferentiated cultures revealed a trace amount of β-tubulin and tau protein in the soma and rudimentary neurites of SH-SY5Y cells (Fig. 2A1–3,D, E). The expression levels of these proteins in cultures treated with RA or a cocktail of RA + BDNF showed a significant increase, with their levels in cultures exposed to RA and BDNF exceeding those of RA-treated and control cultures (Fig. 2B1-3-E). In both sets of cultures, there was a prominent rise in the expression of β-tubulin and tau in neurites, which was particularly notable in RA + BDNF differentiated cultures. Analysis of the colocalization of these structural proteins showed a lower index in outgrowths and soma of cells in control cultures as compared to RA + BDNF cultures (Fig. 2F). Similar studies of β-tubulin and MAP2 also revealed increase in their expression associated with differentiation. The MAP2 level was significantly higher in both soma and neurite of cells in RA-treated cultures as compared to RA-BDNF and controls (Fig. 3A1–E). Notably, the baseline colocalization of β-tubulin and MAP2 in controls was higher than the colocalization of β-tubulin with tau, with the colocalization index of MAP2-β-tubulin indistinguishable between controls and RA-BDNF-treated cultures (Figs. 2F and 3F). The results of differentiation-dependent changes in tau, MAP2 and β-tubulin are likely to reflect their developmental engagement in various structural elements and processes in different cellular compartments[42].

Visualizing synaptic markers in SH-SY5Y-derived neurons

The development of an elaborate network of neurites with abundant contacts in RA + BDNF differentiated SH-SY5Y cultures suggests synaptic wiring of cells. To confirm formation of synaptic connections in RA + BDNF differentiated cultures, we have carried out immunostaining on 12-day-old SH-SY5Y cells for pre and postsynaptic

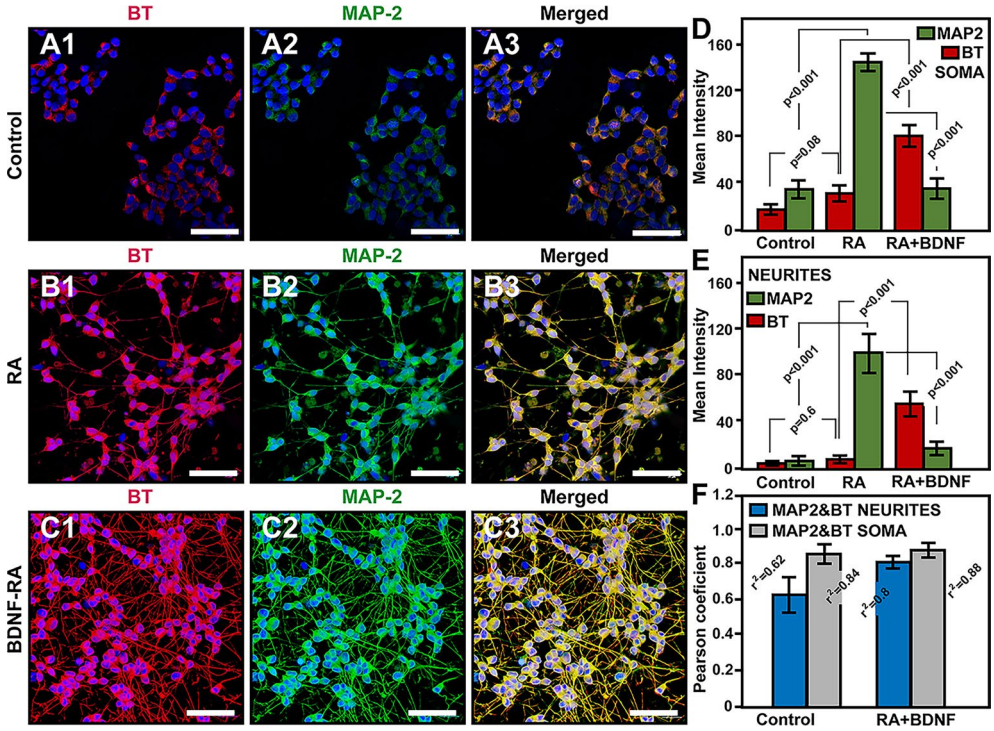

Fig. 3. Quantification of BT – MAP2 expression and distribution in SH-SY5Y cell cultures. (**A1**–**C3**) Typical confocal immunofluorescence micrographs of 12-day-old Control, RA and RA + BDNF cultures stained for β-tubulin (BT) and MAP2 protein (red and green, respectively). Blue - counterstaining of cells with DAPI. Scale bars: 80 µm. (**D**,**E**) Summary histograms of the mean intensity of staining for β-tubulin and MAP2 protein (red and green, respectively) in soma and neurites (SOMA and NEURITES) showing their distribution in Control, RA and RA + BDNF cultures. Histograms show ± SEM. $N = 30$ ROI per group, three replicas. (**F**) The bar graphs show the Pearson correlation values of β-tubulin and MAP2 protein in soma and neurites of control and RA-BDNF differentiated cells. Analysis of the significance of the relationship between the two variables of each dataset with a paired Student *t*-test produced $p < 0.05$ for all datasets.

markers and dendrite-specific protein MAP2[17,36]. Figure 4 demonstrates representative confocal micrographs and summarises the results of the colocalization studies (A-D and E, F, respectively). We used a combination of immunostaining for MAP2 and ubiquitous presynaptic protein synapsin, as well as a combination of MAP2 and a key element of the postsynaptic scaffold of glutamatergic synapses, PSD95[36,43]. In all double-labelled specimens, MAP2-PSD95 and MAP2-synapsin expression was visible in soma and neurites, with abundant juxta-cellular PSD95 or synapsin positive puncta and varicosities also visible (Fig. A1–A3 and B1–B3). While PSD95 puncta were mainly positioned at (or colocalized with) MAP2, there were also numerous PSD-95 or synapsin-positive puncta unrelated to MAP2. Closer scrutiny of double-labelled puncta showed organized arrangements of synaptic markers with MAP2, with the latter known to be associated with dendrites[36,44]. To more rigorously characterize the labelling of putative synapses, after visualizing morphological contacts on brightfield mode, they were scanned in confocal mode, with colocalization analysis conducted using ROIs as specified in Methods (Fig. 4E, F). Measurements of the colocalization index of PSD95, synapsin, and MAP2 revealed a high degree of superposition between MAP2 and PSD95, and a lesser degree of superposition between MAP2 and synapsin in the ROIs corresponding to neurite contacts. This agrees with PSD95 and MAP2 being enriched in dendritic compartments of SH-SY5Y-derived human neurons[45]. The results of our confocal microscopy of SY-SY5Y-derived neurons confirm effective differentiation of RA + BDNF-treated SH-SY5Y progenitors into neurons expressing specific synaptic markers. The nature of neurotransmission and the mediators operating at contacts is a subject of our ongoing experiments.

Spontaneous and evoked calcium dynamics in SH-SY5Y cells

To investigate if structural and molecular differentiation of SH-SY5Y cells into neurons is accompanied by activity changes, we studied spontaneous and evoked Ca^{2+} dynamics using live imaging with Fluo-4 Ca^{2+} sensor. We compared Ca^{2+} dynamics of undifferentiated SH-SY5Y cultures with starved SH-SY5Y cultures or cultures treated with RA or RA + BDNF (Table 2, see also Methods). We observed significant differences in spontaneous Ca^{2+} dynamics with the switch of activity depending on the differentiation state. Figure 5 summarises the results of these experiments with corresponding frequency, amplitude and dye uptake distribution graphs. In control SH-SY5Y cultures, over ~ 70% of cells showed high-amplitude slow oscillation of Ca^{2+}, with the remaining cells exhibiting random transients or keeping in a resting state (Fig. 5A, E–G).

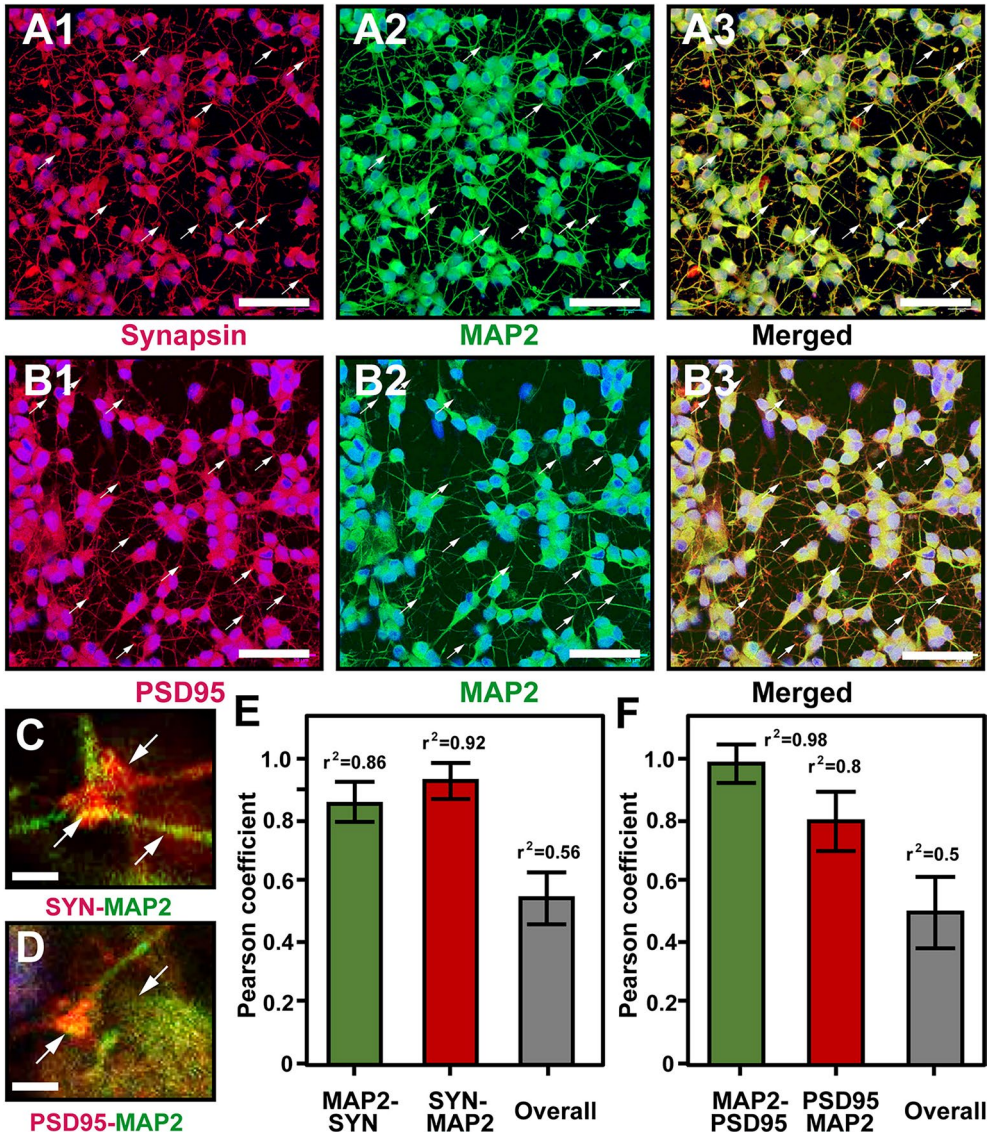

Fig. 4. Expression and localisation of synaptic proteins in RA + BDNF-differentiated cultures. (**A1**–**B3**) Typical confocal immunofluorescence micrographs of 12-day-old RA + BDNF cultures triple-stained for synapsin, MAP2 and DAPI (red, green and blue, respectively). Arrowheads point to putative synaptic contacts. Scale bars: 80 µm. (**C**,**D**) Zoomed-in image of putative synaptic contacts double-stained for synapsin-MAP2 and PSD95-MAP2, respectively. Scale bars: 3 µm. (**E**,**F**) Summary histograms of the colocalization index of synapsin-MAP2 and PSD95-MAP2 show the degree of colocalization of these specific neuronal markers. Histograms show ± SEM. $N = 30$ ROI per group, three replicas. Analysis of the significance of the relationship between the two variables of each dataset with a paired Student t-test produced $p < 0.05$ for all datasets.

Given that FBS deprivation of SH-SY5Y cells promotes their differentiation and increases the expression of neuronal proteins[46,47], we investigated whether a switch in Ca^{2+} dynamics accompanies these changes. In cultures under starvation, high-amplitude regular Ca^{2+} oscillations switched into less regular, low-amplitude transients, with occasional sharp spikes superimposed onto different phases of slow Ca^{2+} waves (Fig. 5A, B,E, F). In the RA group, we observed a dramatic reduction of Ca^{2+} activity, with elimination of high-amplitude spontaneous Ca^{2+} waves (Fig. 5C, E and F). The level of baseline noise was, however, elevated, with occasional low-amplitude transients visible. Importantly, in 12-day-old cultures differentiated with RA + BDNF, we observed a resurgence of low amplitude and random Ca^{2+} transients (Fig. 5D–F). Measurements of the Fluo-4 uptake by SH-SY5Y cells under different experimental conditions revealed considerable differences between various experimental groups, with the uptake of Fluo-4 highest in RA + BDNF-treated cultures and starved groups, as opposed to the lowest uptake in RA-treated SH-SY5Y cultures (Fig. 5G).

To determine if different conditions of SH-SY5Y cultures also affect the stimulation-induced Ca^{2+} transients, we performed live calcium imaging before and under stimulation of cells with carbachol and ionomycin (Fig. 6). Both compounds are known to induce rise of intracellular Ca^{2+} but via different mechanisms[34,48,49]. The choice of concentrations of carbachol and ionomycin was based on published literature[34,50]. Figure 6A–D presents

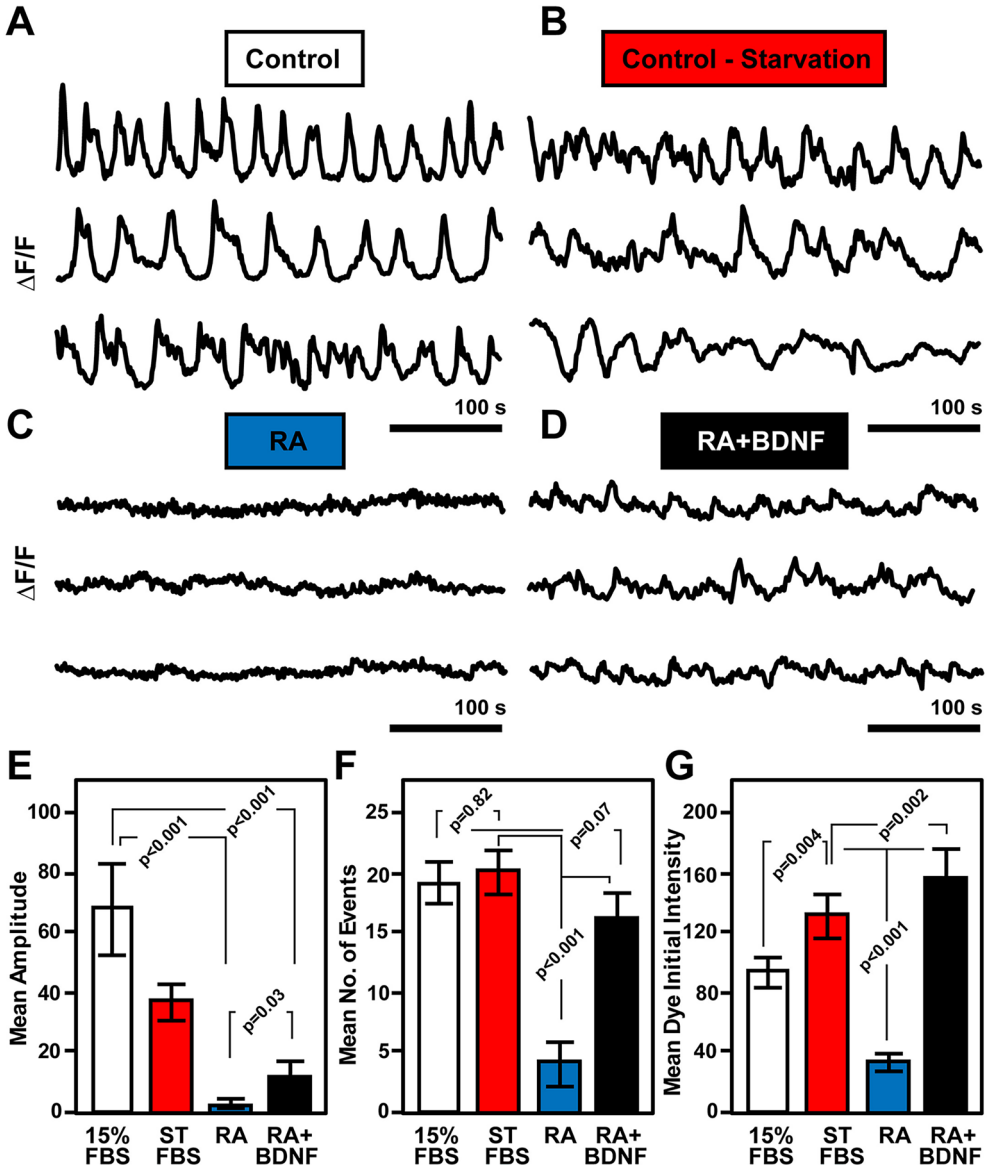

Fig. 5. Live imaging of spontaneous Ca^{2+} dynamics in undifferentiated controls, FBS-starved, RA and RA-BDNF differentiated cells. (**A**–**D**) Raw recording traces of Ca^{2+} dynamics from the soma of three representative cells from each experimental group were collected over 400 s in time series recording mode. Slow high-amplitude oscillations in undifferentiated SH-SY5Y cells (Controls) were rendered less regular and of variable amplitudes by FBS starvation (Control-Starvation) (**A**,**B**). (**C**) Treatment of cells in RA abolished the oscillatory activity, leaving sparse low-amplitude transients, while (**D**) cultures maintained in RA + BDNF showed random and low-amplitude Ca^{2+} transients. (**E**–**G**) Summary histogram of the amplitude and recorded number of events (frequency) in four experimental groups: Control undifferentiated with 15% FBS (white), Control FBS Starved (ST, red), RA (blue) and RA + BDNF (black). (**G**) Histograms of the initial dye uptake in four experimental groups. Histograms show ± SEM. $N = 3$ per group, with at least 30 cells in each group from three repeats.

typical recordings of evoked Ca^{2+} transients with corresponding summary graphs of the amplitude distribution. As can be seen, the application of carbochol in all experimental sets of cultures induced a rapid rise of Ca^{2+} followed by its decline. Analysis of the evoked response amplitude showed that the peak response was highest in RA + BDNF-treated cultures, with amplitudes of control, starved and RA groups remaining within a similar range (Fig. 6A, C). There were also subtle differences in the kinetics of the Ca^{2+} transient decay, with RA and RA + BDNF differentiated cultures showing faster decline (Fig. 6A). The response of cells to ionomycin was consistent across all groups, with evoked Ca^{2+} transients displaying a slower rise with a much broader peak and slower decline (Fig. 6B, D).

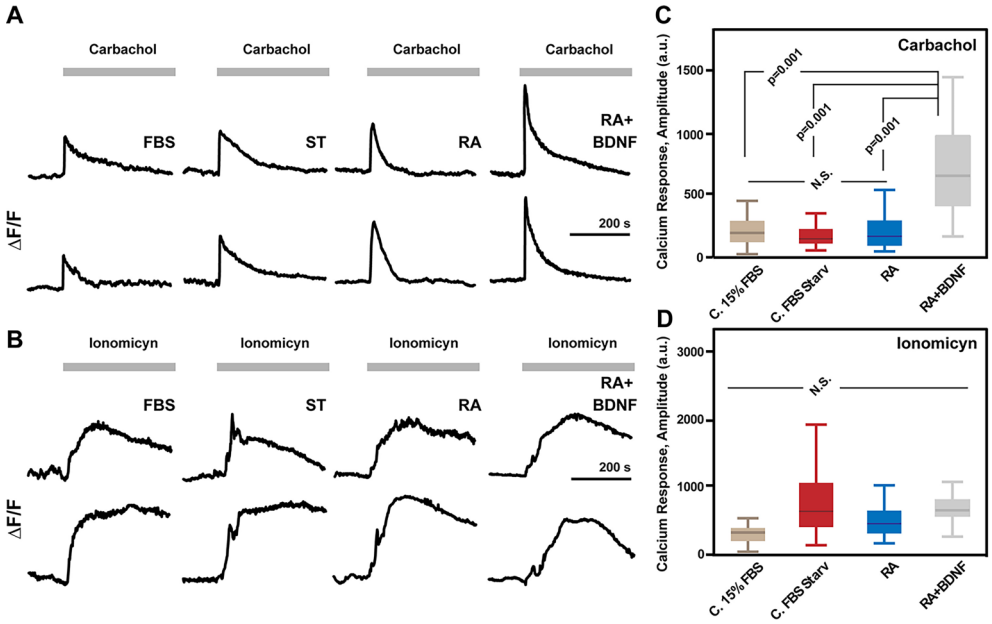

Fig. 6. Live imaging of Ca^{2+} transients in undifferentiated controls, FBS starved, RA and RA-BDNF differentiated cells evoked by carbachol and ionomycin. (**A**,**B**) Typical recordings of evoked by carbochol (**A**) and ionomycin (**B**) Ca^{2+} transients in Undifferentiated SH-SY5Y cells with 15% FBS, Starved (ST) RA and RA + BDNF. The grey bar above recordings indicates the time of the application of stimulants. Note the amplitude and kinetics differences of evoked Ca^{2+} transients in different experimental groups. (**C**,**D**) Box plots summarise the peak amplitude distribution of evoked response in undifferentiated or 15% FBS, FBS starved, RA and RA + BDNF group cultures stimulated by carbachol or ionomycin, respectively. *NS* non-significant.

Discussion

Neuronal differentiation and maturation play a crucial role in the development and function of the nervous system. Overwhelming data suggests specific histochemical, molecular and biochemical alterations in neurons at various stages of their development[26,36,51–57]. However, a significant gap remains in understanding how these changes relate to the developmental adjustments of intrinsic and synaptic activity. In this study, we investigated whether spontaneous and evoked Ca^{2+} dynamics change in developing SH-SY5Y-derived neurons in vitro. In general, the molecular and morphological characteristics of differentiating SH-SY5Y cells observed in our experiments agree with those reported previously[23,46,58,59]. The results of live Ca^{2+} imaging are novel and present a significant milestone in elucidating functional changes accompanying structural and molecular remodeling of neurons derived from SH-SY5Y progenitors.

Like in earlier studies, serum deprivation of SH-SY5Y cells in our experiments set cultures on a differentiation path, initiating polarization of cells with outgrowth of rudimentary neurites [38,47]. Supplementing RA in culture media promoted the elongation of neurites and increased the expression of structural proteins such as β-tubulin, MAP2, and tau, arrested G1 and G2 phases, leading to block of cell proliferation[15,17,60,61]. This process was promoted further by adding BDNF to the cultures, which is known to facilitate the polarisation and differentiation of SH-SY5Y cells[17,18,62]. The polarization of cells was accompanied by the development of dense branches of neurites with increase in the level of tau protein and synaptic markers. Interestingly, RA alone enhanced the MAP2 signal in SH-SY5Y cells more than in combination with BDNF, whereas the combination of RA and BDNF enhanced both MAP2 and tau expression. A possible explanation for this differential response could be that under RA, the rate of neurite growth is slower than that in the presence of BDNF, leading to stronger enrichment of the soma and rudimentary neurites with MAP2.

Because neuronal differentiation and integration into functional networks depend on their electrical activity, which drives release of signaling molecules[57,63–65], we investigated Ca^{2+} dynamics in SH-SY5Y cells at various differentiation stages. Under our settings, the undifferentiated cells show high-amplitude spontaneous Ca^{2+} oscillations and smaller evoked Ca^{2+} transients, also reported in other dividing cells[66,67]. Ample data suggest that the rise in cytosolic free Ca^{2+} caused by its release from endoplasmic reticulum and mitochondria could play a pivotal role in cell proliferation[68–71]. Our imaging experiments show high-amplitude low-frequency Ca^{2+} oscillations in SH-SY5Y cells in the control environment, where they are maintained in active proliferation state, a process involving the activity of Ca^{2+}-calmodulin complex[66,72]. The high-amplitude waves of intracellular Ca^{2+} are essential for the control of cell cycle progression, contributing to several aspects of cell division, including nuclear envelope breakdown and reformation, microtubule activity and cytoskeletal remodelling in the course of cell division[73–75]. They also play a crucial role in controlling molecular motors, driving cell division and migration[76–78]. Importantly, in cultures maintained in serum-deprived conditions, we observed a significant increase in the neurite outgrowth and expression of markers of mature neurons.

The attenuation of large-amplitude Ca^{2+} oscillations in SH-SY5Y cells under starvation and their nearly complete block under RA treatment agrees with the switch of cells from the undifferentiated state onto the differentiation path[30,79]. The latter is in line with increased expression of specific structural proteins such as tau, MAP2 and β-tubulin, stabilising neurites and developing neural networks[80,81]. The abolition of spontaneous high-amplitude Ca^{2+} oscillations by RA agrees with reports showing inhibition of voltage-gated calcium currents by retinoic acid[82,83]. It remains to be shown how supression of calcium dynamics contributes to setting SH-SY5Y cells on the path of differentiation into neurons. The remaining random and rapid Ca^{2+} transients in starved cultures possibly reflect the emergence of rudimentary neuronal activity[57,84]. With further differentiation of SH-SY5Y cells into neurons by a cocktail of RA + BDNF, the residual Ca^{2+} oscillations might reflect specific neuronal processes which are likely to contribute to electro-chemical integration of developing neurons into neural networks[57,85–87].

The results of the analysis of evoked Ca^{2+} transients by carbachol are consistent with the developmental switch of the signalling mechanisms and functions in SH-SY5Y cells. Low amplitude carbachol-induced Ca^{2+} transients in undifferentiated and starved cells suggest limited expression of cholinergic receptors and their weaker coupling with intracellular Ca^{2+} stores[88–91]. In contrast, RA + BDNF-treated SH-SY5Y cells showed a response with the highest amplitude, indicating higher expression of cholinergic receptors and their more effective coupling with intracellular Ca^{2+} stores. The rapid onset of the evoked Ca^{2+} response is likely to involve also depolarisation and influx of this cation via voltage-gated mechanisms. At the same time, the protracted phase can be attributed to the release of Ca^{2+} from intracellular stores[88,90–92]. Accordingly, SH-SY5Y cells are known to express nicotinic (α3,5 and 7, and β2 and 4) and muscarinic (M1/2) receptors[93,94]. Alterations in their levels and signaling mechanisms during differentiation can significantly affect cellular response to acetylcholine and its analogues such as carbochol[95]. Unlike carbochol acting on cholinergic receptors, ionomycin is a calcium ionophore, which enables passage of Ca^{2+} across the plasma membrane without activation of specific receptors or transport mechanisms[48]. The similar amplitude-kinetic characteristics of Ca^{2+} transients evoked by ionomycin in SH-SY5Y cells across all experimental groups agree with non-specific mechanisms of the induction of calcium transients by this ionophore[34,48]. Taken together, these results show that the developmental switch of signalling in SH-SY5Y cells involves both spontaneous and evoked Ca^{2+} dinamics, with potential functional implications.

In conclusion, the results of our experiments demonstrate for the first time that during sequential differentiation of SH-SY5Y cells into human neurons, structural and molecular changes are accompanied by switch of Ca^{2+} activity. The impact of the changes of intrinsic and evoked Ca^{2+} dynamics on molecular and structural alterations and their functional significance for SH-SY5Y-derived neurons remains unclear and is a subject of future studies.

Data availability

The data that support the findings of this study are available from the corresponding author upon reasonable request.

Received: 26 May 2025; Accepted: 8 August 2025
Published online: 01 October 2025

References

1. Moon, C. New insights into and emerging roles of animal models for neurological disorders. *Int. J. Mol. Sci.* **23** (2022).
2. Jucker, M. The benefits and limitations of animal models for translational research in neurodegenerative diseases. *Nat. Med.* **16**, 1210–1214 (2010).
3. Zakowski, W. *Animal Use in Neurobiological Research* 4331–10 (Neuroscience, 2020).
4. Park, S. J. et al. Advancements in human embryonic stem cell research: clinical applications and ethical issues. *Tissue Eng. Regen Med.* **21**, 379–394 (2024).
5. Zhu, Z. & Huangfu, D. Human pluripotent stem cells: an emerging model in developmental biology. *Development* **140**, 705–717 (2013).
6. Keller, J. M. & Frega, M. Past, present, and future of neuronal models in vitro. *Adv. Neurobiol.* **22**, 3–17 (2019).
7. King, N. M. & Perrin, J. Ethical issues in stem cell research and therapy. *Stem Cell. Res. Ther.* **5**, 85 (2014).
8. Medvedev, S. P., Shevchenko, A. I. & Zakian, S. M. Induced pluripotent stem cells: problems and advantages when applying them in regenerative medicine. *Acta Naturae*. **2**, 18–28 (2010).
9. Engle, S. J., Blaha, L. & Kleiman, R. J. Best practices for translational disease modeling using human iPSC-Derived neurons. *Neuron* **100**, 783–797 (2018).
10. Hara, K. et al. Neural progenitor NT2N cell lines from teratocarcinoma for transplantation therapy in stroke. *Prog Neurobiol.* **85**, 318–334 (2008).
11. Xicoy, H., Wieringa, B. & Martens, G. J. The SH-SY5Y cell line in parkinson's disease research: a systematic review. *Mol. Neurodegener.* **12**, 10 (2017).
12. Westerink, R. H. & Ewing, A. G. The PC12 cell as model for neurosecretion. *Acta Physiol. (Oxf).* **192**, 273–285 (2008).
13. Xu, C. & Loew, L. M. Activation of phospholipase C increases intramembrane electric fields in N1E-115 neuroblastoma cells. *Biophys. J.* **84**, 4144–4156 (2003).
14. Tojima, T., Yamane, Y., Takahashi, M. & Ito, E. Acquisition of neuronal proteins during differentiation of NG108-15 cells. *Neurosci. Res.* **37**, 153–161 (2000).
15. Encinas, M. et al. Sequential treatment of SH-SY5Y cells with retinoic acid and brain-derived neurotrophic factor gives rise to fully differentiated, neurotrophic factor-dependent, human neuron-like cells. *J. Neurochem.* **75**, 991–1003 (2000).
16. Korecka, J. A. et al. Phenotypic characterization of retinoic acid differentiated SH-SY5Y cells by transcriptional profiling. *PLoS One*. **8**, e63862 (2013).
17. Hromadkova, L. et al. Brain-derived neurotrophic factor (BDNF) promotes molecular polarization and differentiation of immature neuroblastoma cells into definitive neurons. *Biochim. Biophys. Acta Mol. Cell. Res.* **1867**, 118737 (2020).
18. Riegerova, P. et al. Expression and localization of AbetaPP in SH-SY5Y cells depends on differentiation state. *J. Alzheimers Dis.* **82**, 485–491 (2021).

19. Martinez, M. A. et al. Use of human neuroblastoma SH-SY5Y cells to evaluate glyphosate-induced effects on oxidative stress, neuronal development and cell death signaling pathways. *Environ. Int.* **135**, 105414 (2020).
20. Cohen, N., Betts, D. R., Rechavi, G., Amariglio, N. & Trakhtenbrot, L. Clonal expansion and not cell interconversion is the basis for the neuroblast and nonneuronal types of the SK-N-SH neuroblastoma cell line. *Cancer Genet. Cytogenet.* **143**, 80–84 (2003).
21. Alrashidi, H., Eaton, S. & Heales, S. Biochemical characterization of proliferative and differentiated SH-SY5Y cell line as a model for parkinson's disease. *Neurochem Int.* **145**, 105009 (2021).
22. Forster, J. I. et al. Characterization of differentiated SH-SY5Y as neuronal screening model reveals increased oxidative vulnerability. *J. Biomol. Screen.* **21**, 496–509 (2016).
23. Kaya, Z. B. et al. Optimizing SH-SY5Y cell culture: exploring the beneficial effects of an alternative media supplement on cell proliferation and viability. *Sci. Rep.* **14**, 4775 (2024).
24. Gordon, J., Amini, S. & White, M. K. General overview of neuronal cell culture. *Methods Mol. Biol.* **1078**, 1–8 (2013).
25. Sahu, M. P., Nikkila, O., Lagas, S., Kolehmainen, S. & Castren, E. Culturing primary neurons from rat hippocampus and cortex. *Neuronal Signal.* **3**, NS20180207 (2019).
26. Takano, T., Xu, C., Funahashi, Y., Namba, T. & Kaibuchi, K. Neuronal polarization. *Development* **142**, 2088–2093 (2015).
27. Wainio-Theberge, S., Wolff, A. & Northoff, G. Dynamic relationships between spontaneous and evoked electrophysiological activity. *Commun. Biol.* **4**, 741 (2021).
28. D'Aloia, A. et al. A new advanced cellular model of functional cholinergic-like neurons developed by reprogramming the human SH-SY5Y neuroblastoma cell line. *Cell. Death Discov.* **10**, 24 (2024).
29. Arpana Arjun, R. P., McKinney, G. & Panagiotakos Calcium and activity-dependent signaling in the developing cerebral cortex. *Development* **149** (2022).
30. Berridge, M. J., Bootman, M. D. & Roderick, H. L. Calcium signalling: dynamics, homeostasis and remodelling. *Nat. Rev. Mol. Cell. Biol.* **4**, 517–529 (2003).
31. Bilginer, K. R. & Arslan, Y. A. Exploring neuronal differentiation profiles in SH-SY5Y cells through magnetic levitation analysis. *ACS Omega.* **9**, 14955–14962 (2024).
32. Noble, M. D., Brown, T. H. & Peacock, J. H. Regulation of acetylcholine receptor levels by a cholinergic agonist in mouse muscle cell cultures. *Proc. Natl. Acad. Sci. U S A.* **75**, 3488–3492 (1978).
33. Nakamura, S. et al. Ionomycin-induced calcium influx induces neurite degeneration in mouse neuroblastoma cells: analysis of a time-lapse live cell imaging system. *Free Radic Res.* **50**, 1214–1225 (2016).
34. Meng, J. et al. Activation of TRPV1 mediates calcitonin gene-related peptide release, which excites trigeminal sensory neurons and is attenuated by a retargeted botulinum toxin with anti-nociceptive potential. *J. Neurosci.* **29**, 4981–4992 (2009).
35. O'Leary, V. B. et al. Innocuous full-length botulinum neurotoxin targets and promotes the expression of lentiviral vectors in central and autonomic neurons. *Gene Ther.* **18**, 656–665 (2011).
36. Jorratt, P., Ricny, J., Leibold, C. & Ovsepian, S. V. Endogenous modulators of NMDA receptor control dendritic field expansion of cortical neurons. *Mol. Neurobiol.* **60**, 1440–1452 (2023).
37. Cernaianu, G. et al. All-trans retinoic acid arrests neuroblastoma cells in a dormant state. Subsequent nerve growth factor/brain-derived neurotrophic factor treatment adds modest benefit. *J. Pediatr. Surg.* **43**, 1284–1294 (2008).
38. Martin, E. R., Gandawijaya, J. & Oguro-Ando, A. A novel method for generating glutamatergic SH-SY5Y neuron-like cells utilizing B-27 supplement. *Front. Pharmacol.* **13**, 943627 (2022).
39. DeGiosio, R. A. et al. More than a marker: potential pathogenic functions of MAP2. *Front. Mol. Neurosci.* **15**, 974890 (2022).
40. Hausrat, T. J., Radwitz, J., Lombino, F. L., Breiden, P. & Kneussel, M. Alpha- and beta-tubulin isotypes are differentially expressed during brain development. *Dev. Neurobiol.* **81**, 333–350 (2021).
41. Tabeshmehr, P. & Eftekharpour, E. Tau; One Protein, So Many Diseases. *Biology (Basel)* **12** (2023).
42. Pezzini, F. et al. Transcriptomic profiling discloses molecular and cellular events related to neuronal differentiation in SH-SY5Y neuroblastoma cells. *Cell. Mol. Neurobiol.* **37**, 665–682 (2017).
43. Wegner, W., Mott, A. C., Grant, S. G. N., Steffens, H. & Willig, K. I. In vivo STED microscopy visualizes PSD95 sub-structures and morphological changes over several hours in the mouse visual cortex. *Sci. Rep.* **8**, 219 (2018).
44. Caceres, A., Banker, G., Steward, O., Binder, L. & Payne, M. MAP2 is localized to the dendrites of hippocampal neurons which develop in culture. *Brain Res.* **315**, 314–318 (1984).
45. Lee, H. W., Kim, Y., Han, K., Kim, H. & Kim, E. The phosphoinositide 3-phosphatase MTMR2 interacts with PSD-95 and maintains excitatory synapses by modulating endosomal traffic. *J. Neurosci.* **30**, 5508–5518 (2010).
46. Shipley, M. M., Mangold, C. A. & Szpara, M. L. Differentiation of the SH-SY5Y human neuroblastoma cell line. *J. Vis. Exp.* 53193 (2016).
47. Thomson, A. C. et al. The effects of serum removal on gene expression and morphological plasticity markers in differentiated SH-SY5Y cells. *Cell. Mol. Neurobiol.* **42**, 1829–1839 (2022).
48. Dedkova, E. N., Sigova, A. A. & Zinchenko, V. P. Mechanism of action of calcium ionophores on intact cells: ionophore-resistant cells. *Membr. Cell. Biol.* **13**, 357–368 (2000).
49. Luo, D., Broad, L. M., Bird, G. S. & Putney, J. W. Jr. Signaling pathways underlying muscarinic receptor-induced [Ca2+]i oscillations in HEK293 cells. *J. Biol. Chem.* **276**, 5613–5621 (2001).
50. Johenning, F. W. et al. Distinct intracellular calcium transients in neurites and Somata integrate neuronal signals. *J. Neurosci.* **22**, 5344–5353 (2002).
51. Dos Santos, M. G., Gomes, J. R. & Costa, M. D. M. Methods used to achieve different levels of the neuronal differentiation process in SH-SY5Y and Neuro2a cell lines: an integrative review. *Cell. Biol. Int.* **47**, 1883–1894 (2023).
52. Esposito, M. S. et al. Neuronal differentiation in the adult hippocampus recapitulates embryonic development. *J. Neurosci.* **25**, 10074–10086 (2005).
53. Howard, M. J. Mechanisms and perspectives on differentiation of autonomic neurons. *Dev. Biol.* **277**, 271–286 (2005).
54. Namba, T. et al. Pioneering axons regulate neuronal polarization in the developing cerebral cortex. *Neuron* **81**, 814–829 (2014).
55. Yoshimura, T., Arimura, N. & Kaibuchi, K. Signaling networks in neuronal polarization. *J. Neurosci.* **26**, 10626–10630 (2006).
56. Neuner, J. et al. Pathological alpha-synuclein impairs adult-born granule cell development and functional integration in the olfactory bulb. *Nat. Commun.* **5**, 3915 (2014).
57. Ovsepian, S. V. & Vesselkin, N. P. Wiring prior to firing: the evolutionary rise of electrical and chemical modes of synaptic transmission. *Rev. Neurosci.* **25**, 821–832 (2014).
58. Cheung, Y. T. et al. Effects of all-trans-retinoic acid on human SH-SY5Y neuroblastoma as in vitro model in neurotoxicity research. *Neurotoxicology* **30**, 127–135 (2009).
59. Targett, I. L., Crompton, L. A., Conway, M. E. & Craig, T. J. Differentiation of SH-SY5Y neuroblastoma cells using retinoic acid and BDNF: a model for neuronal and synaptic differentiation in neurodegeneration. *Vitro Cell. Dev. Biol. Anim.* **60**, 1058–1067 (2024).
60. Kalinovskii, A. P. et al. Retinoic Acid-Differentiated neuroblastoma SH-SY5Y is an accessible in vitro model to study native human Acid-Sensing ion channels 1a (ASIC1a). *Biology (Basel)* **11** (2022).
61. Simoes, R. F. et al. Refinement of a differentiation protocol using neuroblastoma SH-SY5Y cells for use in neurotoxicology research. *Food Chem. Toxicol.* **149**, 111967 (2021).
62. Langerscheidt, F., Bell-Simons, M. & Zempel, H. Differentiating SH-SY5Y cells into polarized human neurons for studying endogenous and exogenous Tau trafficking: four protocols to obtain neurons with noradrenergic, dopaminergic, and cholinergic properties. *Methods Mol. Biol.* **2754**, 521–532 (2024).

63. Dawitz, J., Kroon, T., Hjorth, J. J. & Meredith, R. M. Functional calcium imaging in developing cortical networks. *J. Vis. Exp.*, (2011).
64. Holliday, J. & Spitzer, N. C. Spontaneous calcium influx and its roles in differentiation of spinal neurons in culture. *Dev. Biol.* **141**, 13–23 (1990).
65. Spitzer, N. C. Electrical activity in early neuronal development. *Nature* **444**, 707–712 (2006).
66. Maslyukov, A., Li, K., Su, X., Kovalchuk, Y. & Garaschuk, O. Spontaneous calcium transients in the immature adult-born neurons of the olfactory bulb. *Cell. Calcium*. **74**, 43–52 (2018).
67. Nugues, C., Helassa, N., Haynes, L. P. & Mitosis focus on calcium. *Front. Physiol.* **13** 951979 (2022).
68. Zhao, G. et al. Mitotic ER-mitochondria contact enhances mitochondrial Ca(2+) influx to promote cell division. *Cell. Rep.* **43**, 114794 (2024).
69. Capiod, T. Cell proliferation, calcium influx and calcium channels. *Biochimie* **93**, 2075–2079 (2011).
70. Raffaello, A., Mammucari, C., Gherardi, G. & Rizzuto, R. Calcium at the center of cell signaling: interplay between Endoplasmic reticulum, mitochondria, and lysosomes. *Trends Biochem. Sci.* **41**, 1035–1049 (2016).
71. Debir, B., Meaney, C., Kohandel, M. & Unlu, M. B. The role of calcium oscillations in the phenotype selection in endothelial cells. *Sci. Rep.* **11**, 23781 (2021).
72. Kahl, C. R. & Means, A. R. Regulation of cell cycle progression by calcium/calmodulin-dependent pathways. *Endocr. Rev.* **24**, 719–736 (2003).
73. Veksler, A. & Gov, N. S. Calcium-actin waves and oscillations of cellular membranes. *Biophys. J.* **97**, 1558–1568 (2009).
74. Davidson, P. M. & Cadot, B. Actin on and around the nucleus. *Trends Cell. Biol.* **31**, 211–223 (2021).
75. Machaca, K. Ca(2+) signaling, genes and the cell cycle. *Cell. Calcium*. **49**, 323–330 (2011).
76. Sokolov, R. A. & Mukhina, I. V. Spontaneous Ca(2+) events are linked to the development of neuronal firing during maturation in mice primary hippocampal culture cells. *Arch. Biochem. Biophys.* **727**, 109330 (2022).
77. Pinto, M. C. et al. Calcium signaling and cell proliferation. *Cell. Signal.* **27**, 2139–2149 (2015).
78. Kapur, N., Mignery, G. A. & Banach, K. Cell cycle-dependent calcium oscillations in mouse embryonic stem cells. *Am. J. Physiol. Cell. Physiol.* **292**, C1510–1518 (2007).
79. Berridge, M. J. Calcium signalling and cell proliferation. *Bioessays* **17**, 491–500 (1995).
80. Deurloo, M. H. S. et al. Rasal1 regulates calcium dependent neuronal maturation by modifying microtubule dynamics. *Cell. Biosci.* **14**, 13 (2024).
81. Mattson, M. P., Murain, M. & Guthrie, P. B. Localized calcium influx orients axon formation in embryonic hippocampal pyramidal neurons. *Brain Res. Dev. Brain Res.* **52**, 201–209 (1990).
82. de Hoog, E., Lukewich, M. K. & Spencer, G. E. Retinoid receptor-based signaling plays a role in voltage-dependent Inhibition of invertebrate voltage-gated Ca(2+) channels. *J. Biol. Chem.* **294**, 10076–10093 (2019).
83. Vesprini, N. D., Dawson, T. F., Yuan, Y., Bruce, D. & Spencer, G. E. Retinoic acid affects calcium signaling in adult molluscan neurons. *J. Neurophysiol.* **113**, 172–181 (2015).
84. Rosenberg, S. S. & Spitzer, N. C. Calcium signaling in neuronal development. *Cold Spring Harb Perspect. Biol.* **3**, a004259 (2011).
85. Cadwell, C. R. et al. Electrophysiological, transcriptomic and morphologic profiling of single neurons using Patch-seq. *Nat. Biotechnol.* **34**, 199–203 (2016).
86. Ovsepian, S. V. The birth of the synapse. *Brain Struct. Funct.* **222**, 3369–3374 (2017).
87. Ramirez-Amaya, V., Marrone, D. F., Gage, F. H., Worley, P. F. & Barnes, C. A. Integration of new neurons into functional neural networks. *J. Neurosci.* **26**, 12237–12241 (2006).
88. Rani, C. S., Schilling, W. P. & Field, J. B. Intracellular Ca2 + mobilization by thyrotropin, carbachol, and adenosine triphosphate in dog thyroid cells. *Endocrinology* **125**, 1889–1897 (1989).
89. Chakraborty, P. et al. Regulation of store-operated Ca(2+) entry by IP(3) receptors independent of their ability to release Ca(2). *Elife* **12** (2023).
90. Wojcikiewicz, R. J., Safrany, S. T., Challiss, R. A., Strupish, J. & Nahorski, S. R. Coupling of muscarinic receptors to the mobilization of intracellular Ca2 + stores in permeabilized SH-SY5Y human neuroblastoma cells. *Biochem. J.* **272**, 269–272 (1990).
91. White, C. & McGeown, J. G. Carbachol triggers RyR-dependent Ca(2+) release via activation of IP(3) receptors in isolated rat gastric myocytes. *J. Physiol.* **542**, 725–733 (2002).
92. Corrales, A., Xu, F., Garavito-Aguilar, Z. V. & Blanck, T. J. Recio-Pinto, isoflurane reduces the carbachol-evoked Ca2 + influx in neuronal cells. *Anesthesiology* **101**, 895–901 (2004).
93. Serres, F. & Carney, S. L. Nicotine regulates SH-SY5Y neuroblastoma cell proliferation through the release of brain-derived neurotrophic factor. *Brain Res.* **1101**, 36–42 (2006).
94. Adem, A., Mattsson, M. E., Nordberg, A. & Pahlman, S. Muscarinic receptors in human SH-SY5Y neuroblastoma cell line: regulation by phorbol ester and retinoic acid-induced differentiation. *Brain Res.* **430**, 235–242 (1987).
95. Kovalevich, J. & Langford, D. Considerations for the use of SH-SY5Y neuroblastoma cells in neurobiology. *Methods Mol. Biol.* **1078**, 9–21 (2013).

Acknowledgements

The project was supported by the Vice Chancellors Award, the University of Greenwich, Innovation Award 2023 and the Research Excellence Framework Program. D.R. acknowledges support from the Swiss National Science Foundation (310030_192757).

Author contributions

Conception and design: DN, SS, IG, SVO; Experimental research and data analysis: DN, SS, IG, SVO; Drafting, revising and critical comments: DN, SS, IG, DR, SS, SVO; Reading and approval of the final version: DN, SS, IG, DR, SS, SVO; Funding and Project management: SVO.

Declarations

Competing interests

The authors declare no competing interests.

Additional information

Correspondence and requests for materials should be addressed to D.R. or S.V.O.